WILEY | Hindawi

Research Article

Failure Mechanism of Anti-Inclined Karst Slope Induced by Underground Multiseam Mining

Nanyun Wang,[1] **Zuliang Zhong** [1,2] **Xinrong Liu,**[1,2] **and Guofu Gao**[3]

[1]*School of Civil Engineering, Chongqing University, Chongqing 400045, China*
[2]*National Joint Engineering Research Center of Geohazards Prevention in the Reservoir Areas, Chongqing 400045, China*
[3]*Chongqing Institute of Geology and Mineral Resources, Chongqing 401120, China*

Correspondence should be addressed to Zuliang Zhong; haiou983@126.com

There occurred a lot of catastrophic landslides in Southwest China karst areas in recent years. This study numerically simulated the failure process of Pusa landslide by distinct element method (UDEC). The Voronoi diagram algorithm was used to discretize the rock blocks in the upper part of the mining area, and the erosion in sliding source area caused by heavy rainfall was simulated by increasing the block density and reducing the joint strength. Results obtained using UDEC matched the failure process recorded by UAV, and the subsidence of monitoring points on the slope surface was well coincident with the InSAR results. The DEM results are as follows: firstly, under the action of underground coal mining, the overlying strata of the mountain deform toward the goaf and the deformation of the stratum increase significantly with the caving of the roof stratum; and the deep karst fissures in the overlying stratum have an important influence on the deformation of the mountain; the upper strata form a subsidence zone along the fissures, expanding the range of tensile fissures. Secondly, due to the excavation and unloading of the rock masses at the leading edge of the sliding area, the extrusion deformation occurs to the outside of the slope, resulting in the critical instability of sliding area. Finally, with the strength decreasing of rock masses and structural planes by heavy rainfall, the stability of the mountain continues to decrease until the sliding area collapses.

1. Introduction

Mining-induced landslide is a research that has been concerned for more than 100 years [1, 2]. With the continuous exploitation of coal resources in mountainous terrain, catastrophic landslides induced by underground coal mining occur frequently, resulting in a large number of economic losses and casualties [3–10]. The failure process and mechanisms of mining-induced landslides are becoming an increasingly important research [11–13].

Although there were several methods for predicting rock movement induced by coal mining, such as influence function methods [14, 15] and physical test [16, 17], there is no doubt that numerical method can reveal the failure process more comprehensively [4, 18]. Finite element method (FEM) has been widely utilized in engineering, but it is more suitable for analyzing small deformation problems rather than large

deformation problems like landslides [19]. On the other hand, discontinuous deformation analysis (DDA) [20] and distinct element method (DEM) [21] can simulate the large deformation of blocks. Do and Wu [13] and Xiong et al. [4] studied a mining-induced rock avalanche at Nattai North, Australia, using DDA and DEM methods, respectively, which verify that DDA and DEM can be applied to clarify the failure process of a mining-induced landslide. UDEC is a mature DEM software, verified by Cui et al. [22] that it can reveal the progressive failure process of Daguangbao landslide induced by Wenchuan earthquake. Meanwhile, compared with the DDA software, the Voronoi diagram algorithm has been successfully applied in UDEC for the stability analysis of different slope failure types [23–25]. With the Voronoi diagram algorithm, the large rock block can be discretized into many small parts, which promotes a more accurate study of mining fracture propagation and sliding surface formation [26].

Furthermore, landslide is a progressive failure process, affected by several environmental factors. A large number of landslides indicate that the impact of heavy rainfall should not be ignored [18, 27, 28]; there are still a few studies about the impact of rainfall on landslide based on DEM. In addition, the unique geological structure of landslide area and the existence of karst fracture zone will reduce the sliding resistance of source area, which further increases the complexity of numerical method analysis [29–32]. Moreover, fault is also a frequent geological structure of rock slope [33]. Because of the broken rock masses near the fault, the hydraulic characteristics of underground rock masses (permeability, porosity, etc.) [34, 35] are strongly affected. When there exist faults near the underground mining activities, fault in some cases has a significant impact on landslides, resulting in some irregular deformation responses. The Pusa landslide induced by underground coal mining in Guizhou Province, China, including heavy rainfall, fault, and complex karst geology, is a perfect candidate to study mining-induced landslide in karst area with heavy rainfall [36]. Although Zhu et al. [37] used DAN3D to study the runout behavior of Pusa landslide, there remains a lack of slope failure mechanism analysis induced by coal mining.

In summary, many researchers have used numerical methods and model tests to study the failure process of mining slopes. In addition to the slope factors such as weathering action, underground mining, karstification, rock mass structure, and lithological, it is also strongly affected by heavy rainfall factors, which has a stronger influence on karst slope. To our knowledge, there are no reports on the mining-induced landslide considering karst fissures, faults, and heavy rainfall in one model. It is necessary to comprehensively consider the above factors to study the instability mechanism of mining slope. In this paper, with the help of the Voronoi diagram algorithm, the UDEC software is used to simulate the Pusa landslide under mining operation. In this numerical model, the ground fissure characteristics before the landslide are considered, and the distribution of the mining areas is investigated. The slope erosion caused by heavy rainfall is simulated by increasing the density of the sliding source area and reducing the joint strength. The research was to reveal the failure mechanism of Pusa landslide, so that it can provide a reference for the evaluation of the long-term stability on mining-induced slopes.

2. Data and Method

The mega landslide in Pusa, Guizhou Province, China, is selected as the research object in this paper. Firstly, a survey involving the basic geological conditions was performed to understand the mechanism of landslide. Secondly, a detailed field investigation was conducted on the karst characteristics of the landslide and the distribution of the mined area, which further clarified the failure mechanism of the landslide. Finally, a discrete element numerical model was utilized to study the damage and contributing factors. In addition, the deformation results of the model were verified by the InSAR data provided by Chen et al. [38].

3. Engineering Geological Conditions

3.1. Geological Setting. Pusa landslide occurred on August 28, 2017, in a village of Zhangjiawan Town, Nayong County, Guizhou Province, China (N26°38′04.55″, E105°26′56.14″) [36]. More than 500000 m^3 rock masses fell down from the mountain ridge, causing 26 deaths. The ridge of the Pusa landslide located at 2170 m a.s.l, and the foot of the mountain located at 1800 m a.s.l. The study area has a subtropical monsoon climate, with an average annual temperature of 14°C and annual precipitation slightly higher than 1200 mm.

As shown in Figure 1, the exposed formations in the study area include: (1) the Longtan Formation of the Upper Permian (P$_2$l), consisting of silty mudstone, argillaceous siltstone, mudstone, and coal seams; (2) the Changxing–Dalong Formation of the Upper Permian (P$_2$c + d), consisting of limestone, argillaceous limestone, and sandy shale; (3) the Yelang Formation of the Lower Triassic (T$_1$y), mainly composed of limestone and marlstone, with a small amount of sandstone and mudstone.

The occurrence of rock layer is 180°∠8°, and the direction angle of the sliding direction is 320°. Based on field investigation, there are four structural planes in the overlying rock masses of slope body. Their occurrences are (1) 110°∠87°, (2) 326°∠86°, (3) 140°∠88°, and (4) 225°∠88°, respectively. According to the investigation by Fan et al. [36] and Chen et al. [38], there existed many long and deep ground fissures at the trailing edge of the mountain before 2015.

There are two faults F1 and F2 in the mining area, which have some effects on the strata and coal seams in the mining area: (1) fault F1 is close to the outside of mountain, belongs to a normal fault, strikes northeast, leans south-north, dips 63°~70°, and is about 1320 m long; (3) fault F2 is close to the inside of mountain, belongs to a reverse fault, strikes northeast, leans south-north, dips 70°~75°, and is about 709 m long.

There exist 6 mineable coal seams in the Longtan Formation, the attitude of which is consistent with that of the strata. From top to bottom, they are No. 6, No. 10, No. 14, No. 16, No. 18, and No. 20 coal seams, respectively. The inclination angle of the coal seams is generally 7-12°. The average thickness of coal seam is about 1.6 m, and the maximum total thickness is 9.6 m.

According to the field survey results, the Pusa landslide is mainly divided into three areas: the source area (zone A in Figure 2), the track-abrasion area (zone B in Figure 2), and the accumulation area (zone C in Figure 2).

The average height of the caving rock mass in the source area (zone A) is about 85 m, the width is about 145 m, the average thickness is about 40 m, and the total volume is about 49.3 × 104 m^3. The upper part of the rear wall is a steep medium-thick-thick limestone with a thickness of about 20 m. Since the lower rock mass has collapsed, two concave cavities have been formed in the lower part of the limestone. There are scratches on the middle and lower rock walls, with an inclination of 305°. The main rock mass near the shear outlet is siltstone and marl. Although it has been affected by multiple groups of structural planes, it still
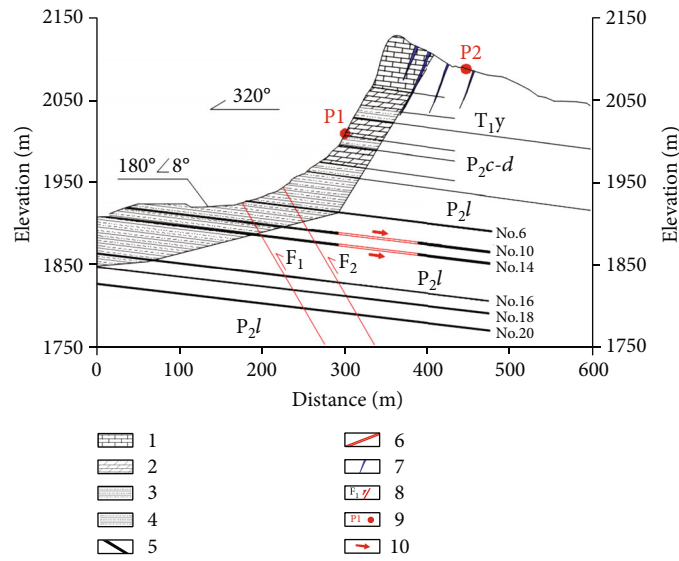
FIGURE 1: Prelandslide longitudinal profile (1-1′ in Figure 4): (1) limestone; (2) marlstone; (3) siltstone; (4) mudstone; (5) coal seam; (6) goaf area; (7) tensile fissure; (8) fault; (9) InSAR monitoring point; (10) mining direction.
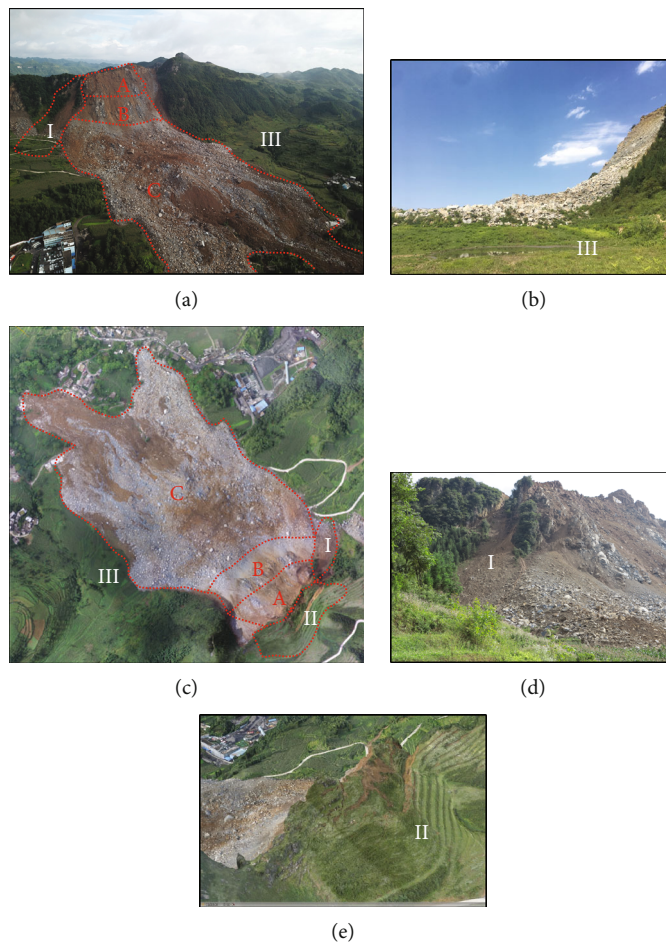

FIGURE 2: Overview of the Pusa landslide: (a) full view; (b) side view; (c) UAV image; (d) deep crack; (e) ground fissures behind the mountain.
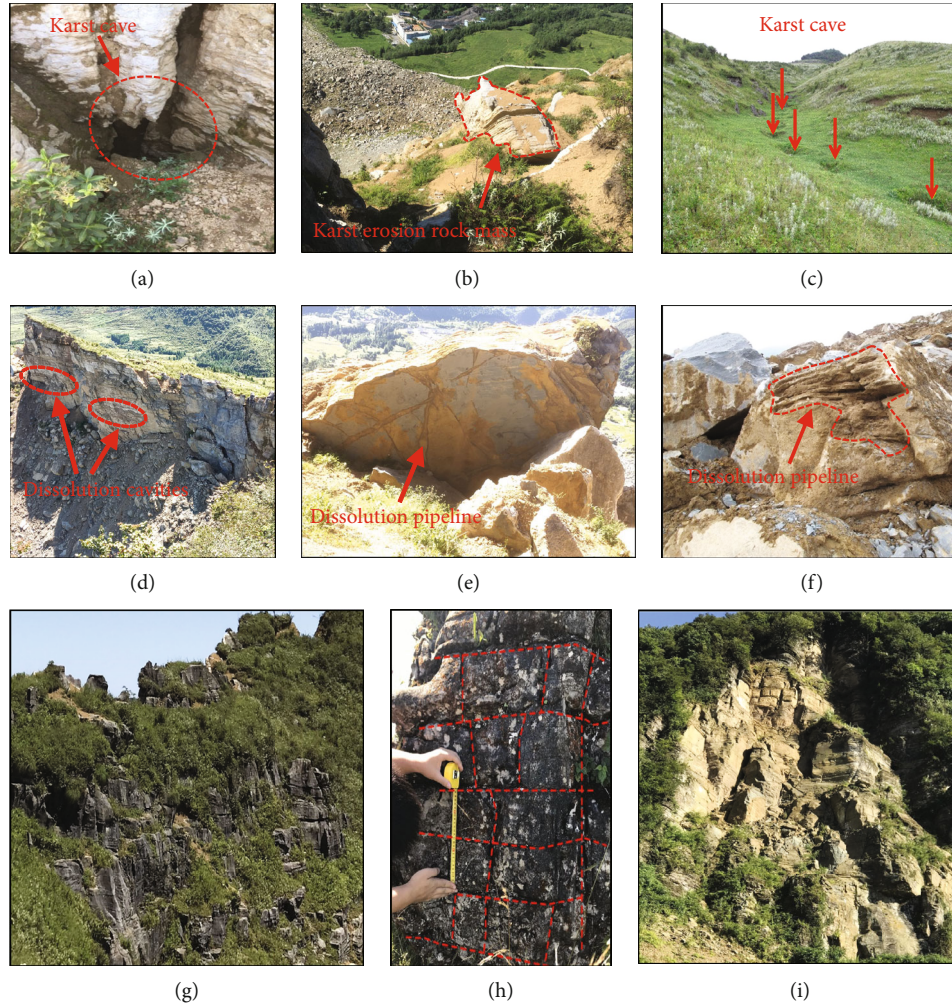
FIGURE 3: Typical erosion signs and rock structure of collapse source area: (a) karst cave; (b) karst erosion rock mass in source area; (c) karst cave behind the mountain; (d) dissolution cavities in sliding surface; (e) dissolution pipeline in source area; (f) dissolution pipeline in deposition area; (g) block structure behind the landslide; (h) joint size of blocks behind the mountain; (i) block structure of local collapse on the left of landslide.

maintains a large block structure. The maximum size of the rock mass in the front and middle of the collapse is $10 \text{ m} \times 10 \text{ m} \times 15 \text{ m}$.

The track-abrasion area is mainly distributed between the elevations of 1920 m and 2030 m. When the unstable rock masses suddenly collapse, the rock scrapes the original loose deposits on the lower slope surface with huge potential and kinetic energy. The scraping action made the steep wall surface in this area retreat about 1.5 m. The track-abrasion area is about 180 m wide and 80 m high, and the track-abrasion area is about $2.1 \times 10^4 \text{ m}^3$.

The deposition area was a relatively open gentle slope area before collapse. The middle part of the deposition area is distributed with a lot of rubble, mainly composed of siltstone and marl. The average length of deposition area is about 575 m, and the width is about 360 m. It is estimated that the thickness of the deposition area is about 1.5 m, and the amount of shovel scraped in the deposition area is about $31 \times 10^4 \text{ m}^3$. After the collapse, a series of tensile fissures with a strike of 35° were produced behind the mountain (zone II in Figure 2). The largest tensile fissure is about 180 m long and 12 m deep, with an opening degree of about 34 m.

As shown in Figure 3, karst features are developed in the limestone layers at the top of the slope, including dissolution cavities, dissolution pipes, and dissolution fissures on the steep cliff walls. A series of dissolution phenomena can be clearly seen in the limestone on the ridge, including the dissolution of the rock out of the cavity, a series of small depressions distributed on the slopes, and the existence of limestone blocks in the accumulation. On the shoulder of the slope (about 2110 m above sea level), four groups of deep and large karst fissures are developed downward (shown in Figure 1), with a depth of 50-80 m and a width of 2-3 m.

3.2. Triggering Factors of Landslide

3.2.1. Coal Mining Activities. The coal mines in the study area mainly adopt inclined shaft development, the strike

longwall retreating mining method is used to mine the mine, and the roof is treated by all caving method. From 2007 to December 2010, No. 16 coal seam was mainly under mining. From 2011 to 2012, the coal mine operation was suspended until No. 14 coal seam was started to mining in November 2013. After the mining of No. 14 coal seam was completed in September 2016, the mining of No. 10 coal seam began and lasted until the Pusa landslide occurred in August 2017. Meanwhile, the width of No. 10 and No. 14 mining areas is 90 m (in 1-1′ cross section), and No. 14 mining area lies directly below No. 10.

3.2.2. Heavy Rainfall. Nayong County has a subtropical monsoon climate, with an annual average temperature of 13.6°C and an annual average rainfall of 1243.9 mm. As shown in Figure 5, the rainfall concentration period is from May to August. From June 21, 2017, to July 21, 2017, the rainfall in the study area increased sharply by 374 mm [36], which further deteriorated the stability of the relatively broken slope affected by goaf, karst fissure, and weathering. Rainwater flows into the slope with joints and fissures at the top, which accelerates the collapse and sliding of the slope from two aspects: (1) resulting in the increase of rock and soil bulk density and (2) promoting the deterioration of mechanical parameters of slope fissures and joints, such as tangential stiffness, tensile strength, cohesion, and internal friction angle [28].

4. Numerical Model

The two-dimensional distinct element code UDEC is widely utilized to study the failure mechanisms of rock slope [39]. In this code, blocks are separated by contacts that are considered analogous to discontinuities in rock masses; the rotation of rock blocks can also be simulated in this software.

4.1. Parameters of Rock Masses and Joints. In this model, the rock masses adopt the classic elastoplastic theory Mohr-Coulomb criterion, and the contacts adopt the Mohr-Coulomb criterion with residual strength. When the contact breaks, the residual strength parameters are used to replace the original mechanical parameters of contact. The simulation of the fracture process of the complete rock masses can restore the failure process of the slope more accurately, so the Voronoi grid division method [25] was used to discretize the block above the mining area, as shown in Figure 6. According to the study by Cui et al. [40], the parameters of rock masses with the Voronoi grid are listed in Table 1. The parameters of rock masses without the Voronoi grid are listed in Table 2. The parameters contacts, including interfaces and joints, can be found in Table 3.

4.2. DEM Model. The DEM model is established based on the cross section in Figure 1. The coal seams below No. 14 coal seam were mined before 2011; No. 10 and No. 14 coal seams were under mining after November 2013. However, the deep and large fractures behind the mountain were all produced before 2013. This means that the deep fissures behind the mountain are caused by the coal mining below
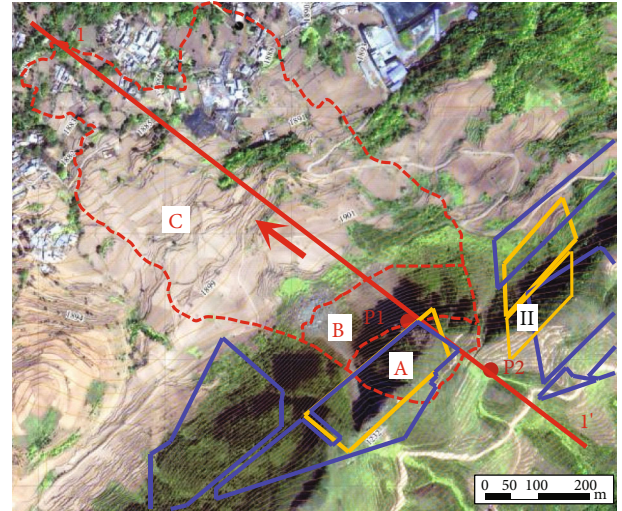
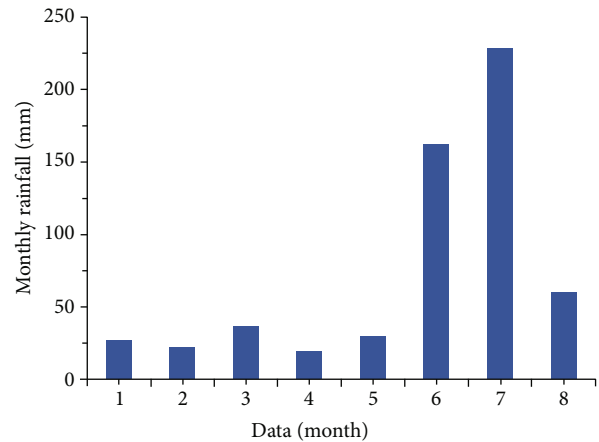FIGURE 4: Top view of No. 10 coal seam goaf, monitoring point, and sliding area.

FIGURE 5: Monthly rainfall preceding the landslide event recorded by the Zhangjiawan Town rainfall station in 2017 [36].

No. 14 coal seam. Four deep fissures have been considered in the numerical model in order to be equivalent to the influence of the coal mining below No. 14 coal seam, so this numerical model before mining is in the actual situation after 2013. Except for No. 10 and No. 14 coal seams, the other coal seams have been mined out for several years before the landslide, so only the mining activities of No. 10 and No. 14 coal seams were analyzed in this model. These four fissures are 50~80 m deep and 1.5 ~ 2 m wide. The No. 14 coal seam is mined first and then the No. 10 coal seam. Each coal seam is set with 9 calculation steps, and each calculation step is 10 m. After the two seams are mined, rainfall conditions are applied to the sliding area. Monitoring points P1 and P2 (as shown in Figures 1 and 4) were monitored by satellites from September 2016 to August 2017 [41].
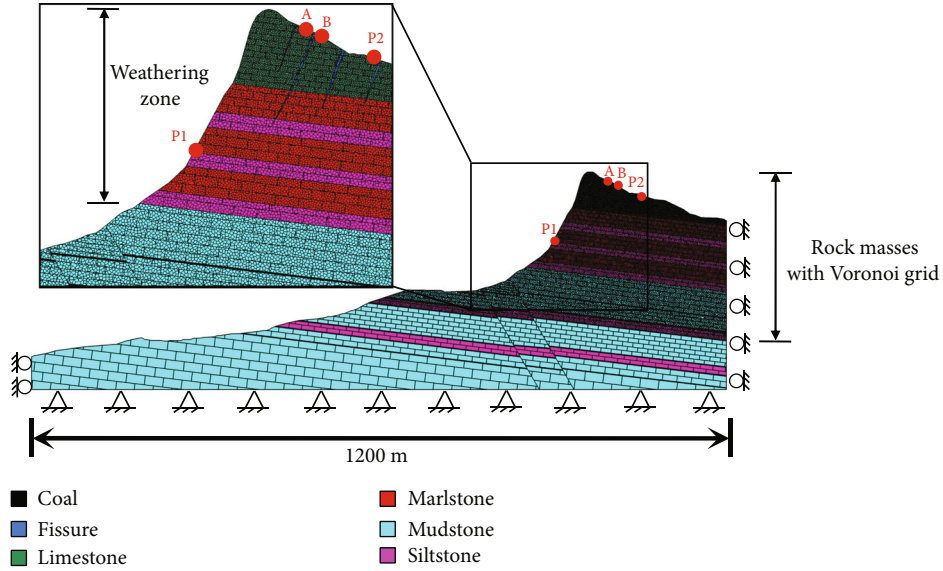
FIGURE 6: Model geometry and boundary conditions.

TABLE 1: Parameters of rock masses with the Voronoi grid.

Lithology		Limestone	Marl	Siltstone	Mudstone	Weathering zone at the slope shoulder	
						Natural	Saturated
Block	Density (kg/m³)	2700	2650	2570	2460	2700	2760
	Bulk modulus (GPa)	15.35	12.86	9.26	5.13	15.35	
	Shear modulus (GPa)	14.11	10.38	7.81	3.23	14.11	
	Cohesion (MPa)	16.2	11.3	10.8	7.8	16.2	
	Friction angle (°)	37	34	35	33	37	
	Tensile strength (MPa)	4.2	2.6	3.6	2.5	4.2	
Joints	Normal stiffness (GPa)	300	100	110	90	300	
	Shear stiffness (GPa)	170	70	90	50	170	
	Cohesion (MPa)	13.2	7.3	5.6	3.6	13.2	
	Friction angle (°)	43	37	33	26	43	
	Tensile strength (MPa)	9.3	5.6	2.6	1.7	9.3	
	Residual cohesion (MPa)	0.11	0.15	0.13	0.11	0.11	
	Residual friction angle (°)	12	13	11	8	12	
	Residual tensile strength (MPa)	0.01	0.01	0.01	0.01	0.01	

TABLE 2: Parameters of rock masses without the Voronoi grid.

Lithology	Density (kg/m³)	Bulk modulus (GPa)	Shear modulus (GPa)	Cohesion (MPa)	Friction angle (°)	Tensile strength (MPa)
Siltstone	2630	12.35	7.13	1.51	35.75	3.40
Mudstone	2450	5.13	3.23	1.24	30.11	2.50
Coal	1350	4.00	2.50	0.52	47.98	0.31
Karst fissure fillings	1800	0.12	0.08	0.12	27	0

In this model, the stratum above No. 14 coal seam is discretized by the Voronoi grid, which will be more conducive to study the stratum movement and the crack expansion above the mining goaf. The influence of karst on the slope is reflected by setting four deep ground fissures and reduction of the parameters in weathering zone. In the field

TABLE 3: Mechanical parameters of the discontinuity surface.

| Lithology	Normal stiffness (GPa)	Shear stiffness (GPa)	Cohesion (MPa)	Friction angle (°)	Tensile strength (MPa)
Coal seam interface	2.8	2.9	0.8	15	0.10
Other interfaces	6.0	6.0	1.2	22	0.15
Fault	4.0	3.5	0.5	15	0
Limestone joint	8.0	6.0	0.25	32	0.05
Marlstone joint	7.0	5.0	0.5	29	0.08
Siltstone joint	6.0	4.0	0.6	23	0.06
Mudstone joint	4.0	3.0	0.32	17	0.03
Weathering zone at the slope shoulder					
Natural	8.0	6.0	0.25	32	0.05
Saturated	6.0	4.0	0.18	26	0.03
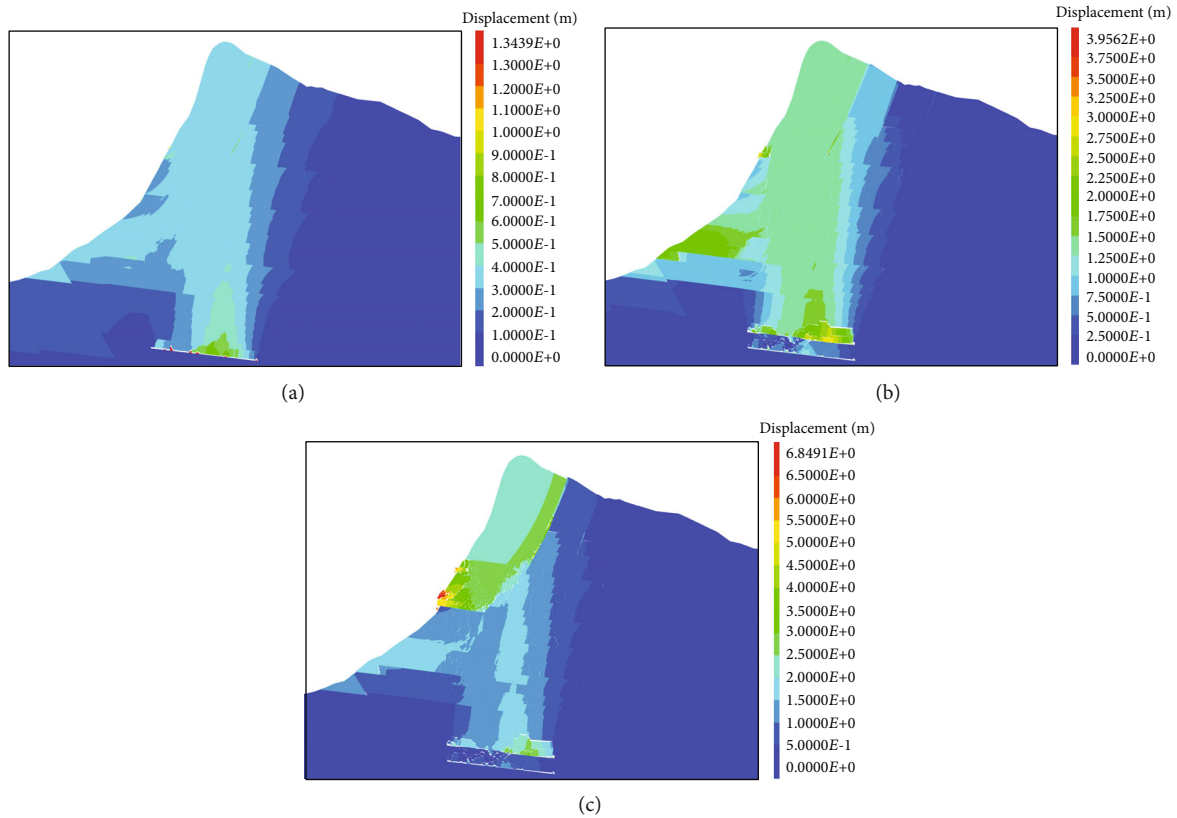
FIGURE 7: Displacement cloud map of mining slope: (a) No. 14 coal seam mined; (b) No. 10 coal seam mined; (c) after heavy rainfall.

investigation, it was found that those four ground fissures (in Figure 1) were filled with many fillings, mainly including broken rock masses and dissolution weathering products. Therefore, the formation of ground fissures is mainly achieved by reducing the block parameters to the filling parameters. The geometry of the numerical model and boundary conditions can be found in Figure 6. It should be noted that point A and point B are, respectively, in the sliding source area and noncollapsing area, and the sliding surface is located between point A and point B.

5. Numerical Results

5.1. Characteristics of Rock Movement. The displacement cloud diagram and velocity vector diagram after coal mining and heavy rainfall are shown in Figures 7 and 8, respectively.

As shown in Figure 7(a), after the No. 14 coal seam was mined, the roof strata caved, and the subsidence basin of the overburden stratum expanded upward in a conical shape. The maximum deformation is roof caving, nearly 1.34 m. When the No. 10 coal seam was mined (Figure 7(b)), the
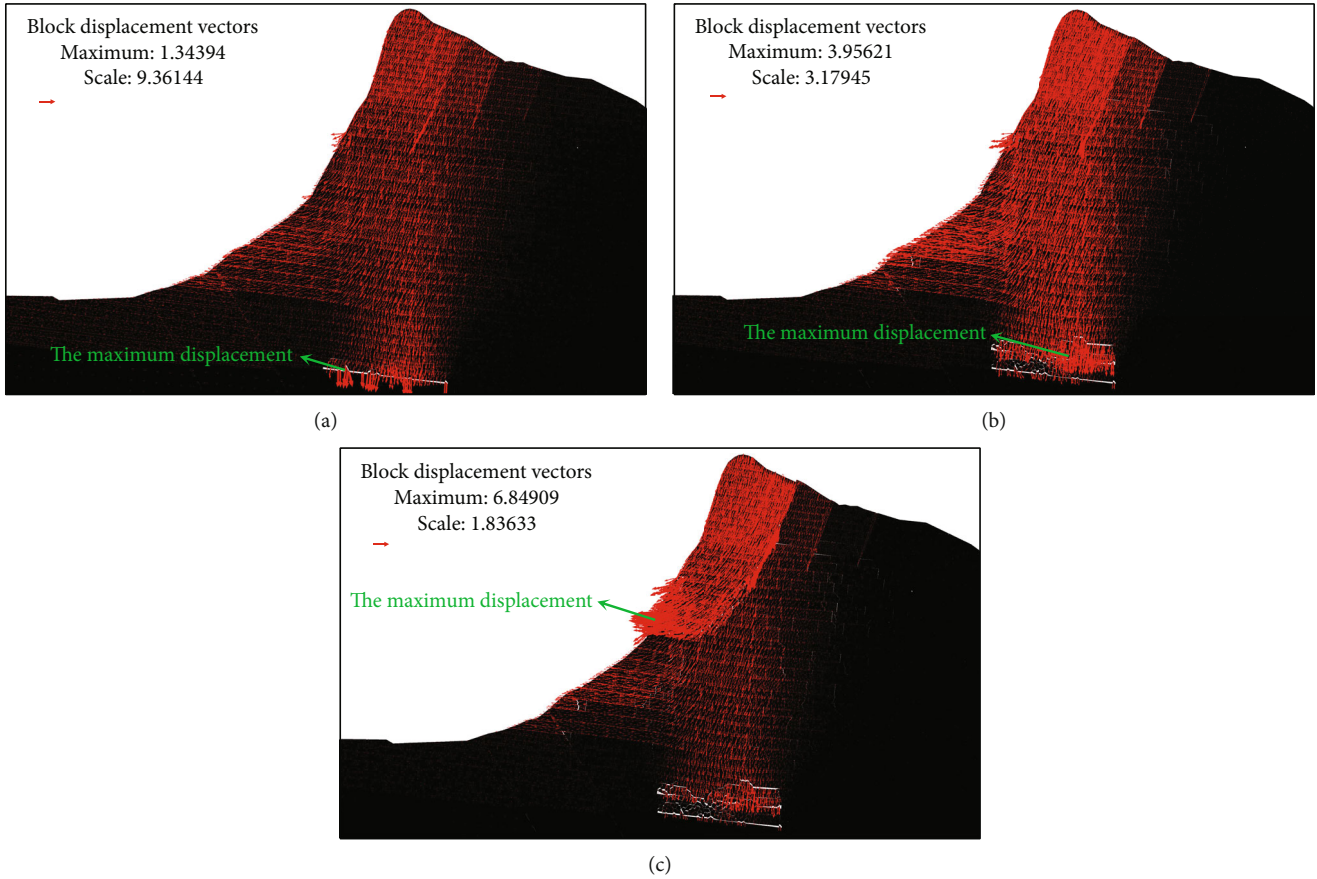
(a)

(b)

(c)

FIGURE 8: Displacement vector diagram: (a) No. 14 coal seam mined; (b) No. 10 coal seam mined; (c) after heavy rainfall.

deformation of overburden stratum was significantly increasing, forming a step-like bending subsidence zone, and continuously sliding along the deep ground fissures. Moreover, the front edge of slope was most affected. The rock masses at the slope toe were extruding out of the slope, which has an important impact on the stability of the mountain. The mining of No. 10 coal seam increases the differential deformation between the potential sliding area and stable area. However, the maximum displacement is about 3.95 m, approximately the same to the thickness of No. 14 and No. 10 coal seam, which indicates that the slope is still stable at this stage. After the heavy rainfall (Figure 7(c)), the differential settlement of the rock masses on both sides of the deep ground fissures increased sharply. The maximum displacement of sliding body is more than 6.8 m, locating at the lower position of the sliding surface.

No. 10 and No. 14 coal seams are located about 250 m directly below the top of the mountain. After the mining of the No. 14 coal seam, roof materials collapse into the mining panel; the upper rock layer bends and deforms, resulting in a maximum displacement of 1.34 m. The moving direction of the rock mass in the sliding source area is parallel to the free surface of the slope, without extruding outwards (shown in Figure 8(a)). However, the rock masses between the sliding source area and the fault are almost horizontally squeezed out. When the No. 10 coal seam was mined, the above phe-
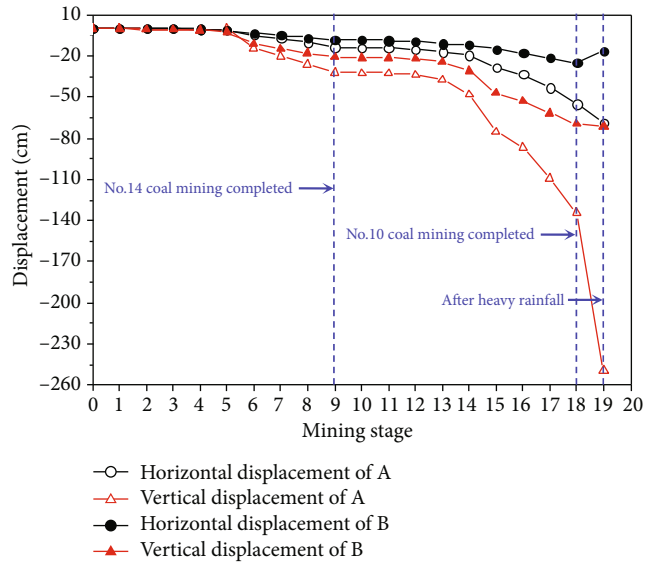

FIGURE 9: Displacement of monitoring points A and B.

nomenon was obviously aggravated, with the maximum moving displacement of 3.96 m, and rock avalanches appeared in part of the rock mass in the sliding area (shown in Figure 8(b)). After the heavy rainfall, the slope was in a critical state of instability, and the rock mass displacement
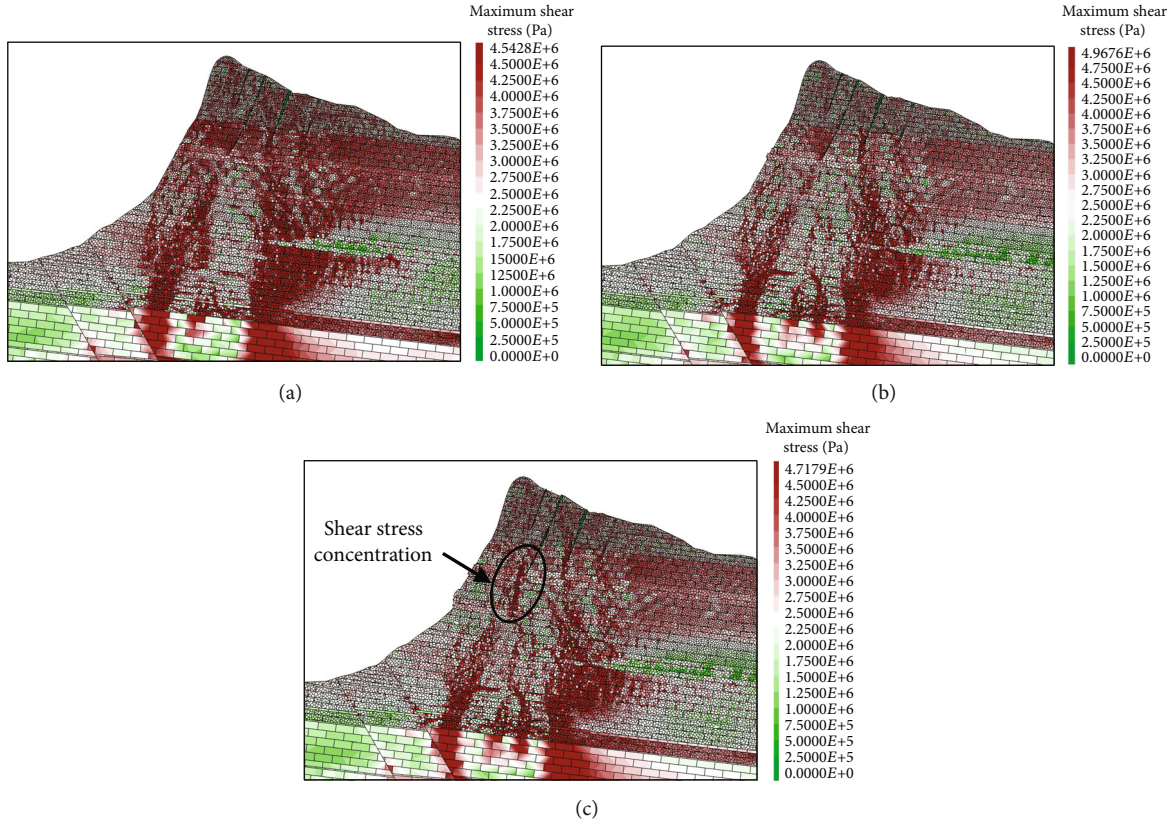
(a)

(b)

(c)

FIGURE 10: Maximum shear stress cloud map of mining slope: (a) No. 14 coal seam mined out; (b) No. 10 coal seam mined out; (c) after heavy rainfall.

in the slid source area increased sharply and squeezed out (shown in Figure 8(c)).

Point A and point B in Figure 6 are selected to analyze the sliding era. Point A is located on the potential sliding body, point B is located behind the potential sliding body, and there is a deep ground fissures between these two points. Therefore, the deformation process of the potential sliding body can be quantitatively described by comparing the relative displacements of point A and point B.

It can be seen from Figure 9 that the horizontal and vertical displacements of point A are both larger than those of point B during coal seam mining and heavy rainfall. The vertical displacements of two monitoring points are always greater than the horizontal displacements at each stage. After the No. 14 coal seam is mined, the horizontal displacement and vertical displacement of point A are 1.6 times and 1.5 times of point B, respectively, the displacements of points A and B are not much different, and the potential sliding surface has not yet formed. When the No. 10 coal seam was mined, the horizontal displacement and vertical displacement of point A are 2.1 times and 1.9 times of point B, respectively, indicating that the potential sliding surface had been formed at this time. With the action of heavy rainfall, the ratio of horizontal and vertical displacements between A and B becomes 4.2 and 3.5, respectively, which means that the sliding body has begun to slide and the slope body has become unstable.

TABLE 4: Vertical displacement comparison between InSAR results and DEM results.

Monitoring points	DEM results	InSAR results	Error (%)
P1	56.2 mm	60.5 mm	7.1
P2	-71.93 mm	-104.2 mm	31

5.2. Characteristics of Stress Evolution. Figure 10 shows the distribution of maximum shear stress in the mining karst mountain. When No. 14 coal seam is mined (Figure 10(a)), the maximum shear stress at both ends of the void area is above 4.5 MPa. There is a large-scale stress redistribution in the karst mountain above the goaf. The roof strata broke due to the lack of support, causing the gravity of overburden rock masses to transfer to both sides of goaf. The pressure relief zone appears above the goaf, and the pressurized zone is formed on both sides of goaf; the pressurized zone extends up to the potential sliding surface.

After the No. 10 coal seam was mined (Figure 10(b)), the maximum shear stress increased to 4.97 MPa, and the height of the pressure relief zone also increased with the thickness of the mined coal seam. This indicates that when the thickness of the mined coal seam is not large, the rock layer above the goaf forms a composite beam structure to bear the overlying load. When the thickness of the mined coal seam increased, the roof strata collapse in a large area. The
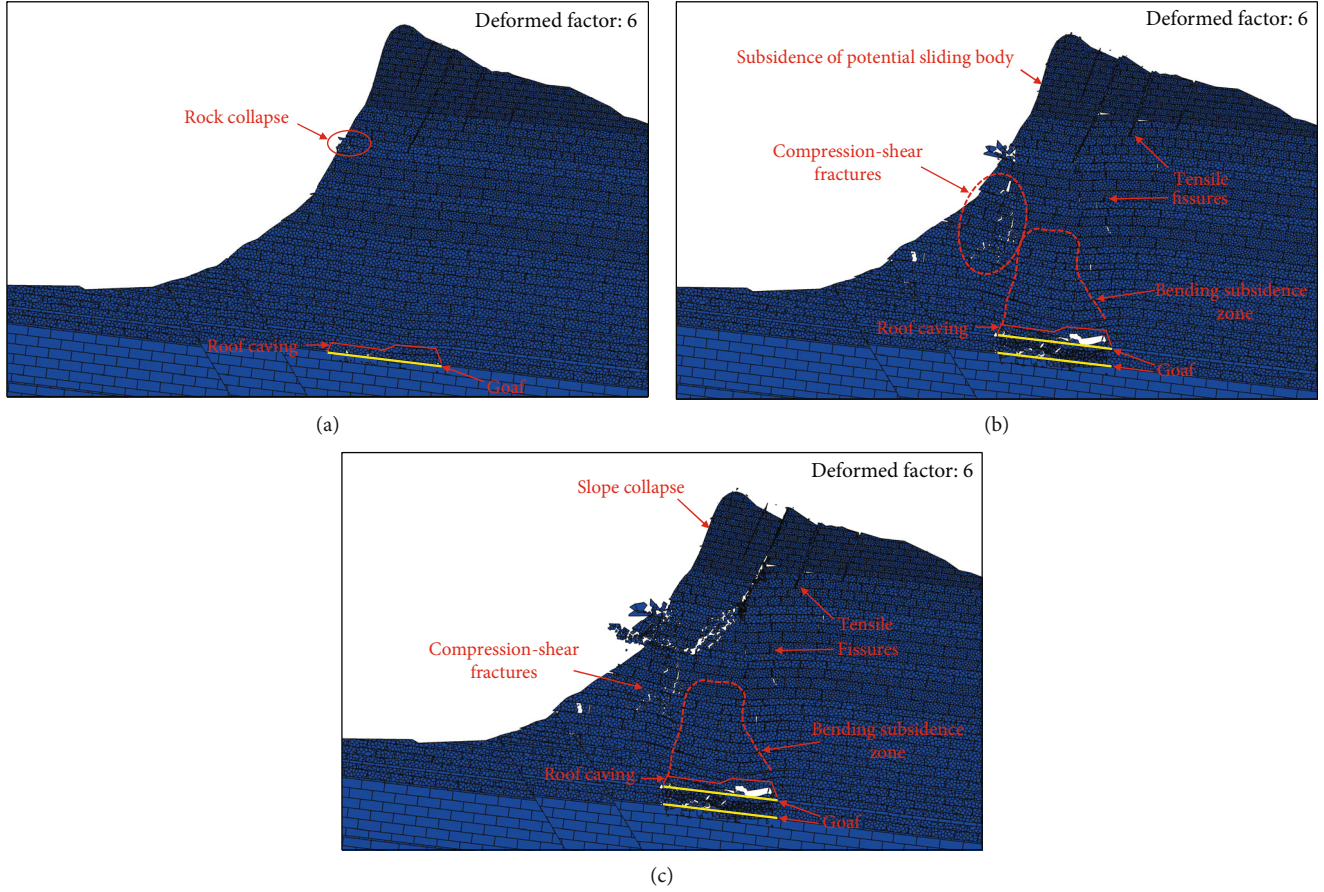
(a)

(b)

(c)

FIGURE 11: The slope failure characteristics after coal seam mining and heavy rainfall: (a) No. 14 coal seam mined out; (b) No. 10 coal seam mined out; (c) after heavy rainfall.

composite beam structure broke due to the large span, lying on the rock masses of the roof caving.

After heavy rainfall (Figure 10(c)), due to the strength reduction of the mechanical parameters of the overlying rock masses and joints, shear stress concentration appears on the potential sliding surface, which means that the sliding surface was slipping.

5.3. Comparison with Preevent Deformation Monitored by InSAR. The Pusa landslide, in Guizhou, China, occurred on 28 August 2017, and the preevent deformation has been recovered by Chen et al. [41] with multisensor synthetic aperture radar (SAR) imagery. The time series of satellite monitoring data is from September 2016 to August 2017; during which, only No. 10 coal seam was under mining (as shown in Figure 4).

To analyze the temporal evolution of the landslide deformation, deformation time series at two points (P1 and P2 in Figures 1 and 4) have been extracted. It should be noted that the monitored deformation is in the line of sight (LOS) direction, and the vertical deformation component can be retrieved as follows [42]:

$$d_v \approx \frac{d_{\text{Los}}^{\text{Desc}} + d_{\text{Los}}^{\text{Asc}}}{2 \cos \theta}, \qquad (1)$$

where d_v is the vertical deformation component; $d_{\text{Los}}^{\text{Desc}}$ and $d_{\text{Los}}^{\text{Asc}}$ are, respectively, the deformation components along the descending and ascending LOS directions; and θ is radar incidence angle. According to research of Li et al. [43], the radar incidence angle is selected as 23°.

Due to the lack of the mining schedule of coal seam, the comparison between the InSAR results and the numerical results is selected after heavy rainfall. The comparisons are listed in Table 4 (positive values represent uplift, and negative values represent sinking down). The InSAR monitoring point P1 is located below the source area, and P2 is located behind the source area. It is clear that the DEM model of the Pusa landslide has a well prediction on the uplift of P1, but the error of prediction on point P2 is 31%.

6. Discussion on Failure Mechanism

The evolution process of rock stratum fissure caused by underground coal mining and heavy rainfall is shown in Figure 11. To represent the phenomenon of rock fissures more clearly, the deformation of the model is amplified by 6 times, that is, the "deformed factor" in Figure 11. The overlying rock stratum after coal seam mining can be regarded as beams or slabs. With the continuous mining activities, the span of goaf is getting wider, causing the increase of the

bending moment at the midspan and the shear force at both ends of the support. When the stress at the most unfavorable position of the rock strata reaches load limit, the rock layer will break or even collapse. After the No. 14 coal seam was mined (Figure 11(a)), the roof strata collapsed, and the overlying rock stratum above the roof appeared a bending subsidence zone. There occurred local rock collapse in front of the slope body, forming a potential sliding surface. When the No. 10 coal seam is mined (Figure 11(b)), the roof caving zone keeps expanding, and the overburden rock stratum above the roof strata continues bending and sinking. There appeared rock layer dislocation near the fault, tensile fissures behind the slope, and compression-shear fractures in front of the slope, forming a potential sliding slope body. After the heavy rainfall (Figure 11(c)), the deformation of the potential sliding body increases sharply. The rock mass at the shoulder of the slope slides down along the deep ground fissure, the rock mass in the middle of the slope collapses and extrudes, and the slope is already unstable and damaged.

In general, based on the numerical simulation analysis of the Pusa landslide, the failure process of the Pusa landslide can be summarized as follows:

(1) Mining operation before 2017 aggravated the deformation of the mountain and the propagation of fissures, resulting in the formation of deep and large fissures on the surface of the slope, which is also more conducive to water infiltration and dissolution development

(2) Due to the superimposed mining disturbance of multiple coal seams, the rock mass at slope toe was squeezed out, the rock layer on the left side of the goaf was pulled apart, and a rock bridge was formed on the slope. The heavy rainfall made part of the ground fissures filled with water; the rock mass was gradually saturated, which increased the weight of sliding area and reduced the strength of the joints. The slope slipped down along the deep fissures and deformed, and the lower rock bridge was crushed and extruded. The slope has an overall dumping destruction

In addition, the study mountain is located on the Yunnan-Guizhou Plateau, and long-term sunshine and temperature differences will accelerate the fragmentation of the rock mass. This is also a factor that cannot be included in the numerical simulations in this paper.

7. Conclusions

In this paper, combined with the field investigation and numerical results, the movement characteristics of the overburden rock stratum and the evolution law of cracks in the Pusa landslide were studied. The failure process and failure mode of karst mountain collapse under the action of underground mining and heavy rainfall are proposed. The following main conclusions are drawn:

(1) In the process of coal seam mining, the slope undergoes three stages: coal seam roof caving, overburden cantilever tension fracture, and overburden overall dumping and settlement. After the heavy rainfall, the source area began to slide, and the slope collapsed as a whole body. The failure mode of the Pusa landslide controlled by deep and large karst fissures can be summarized as slip and extrusion of the leading edge of the mountain, upward transmission of tensile fractures, collapse of the leading edge, and overall dumping

(2) After the coal seam is mined, it is mainly manifested as loading on both sides of goaf and unloading above the goaf. With the continuous advancement of the mining space, the overburden rock layers break and deform, compacting the rock masses in the caving zone, also transferring the goaf clearance space to the sliding area and deep karst fissures

(3) The long-term underground coal seam mining action, karst dissolution, and weathering action make the mountain stay in a critical instability state. The reduction of the mechanical strength of rock masses and structural planes caused by heavy rainfall before the collapse is the direct trigger factor of Pusa landslide

Data Availability

The data used to support the findings of this study are included within the article.

Conflicts of Interest

The authors declare that they have no conflicts of interest.

Acknowledgments

References

[1] D. Cruden and D. Martin, "Before the frank slide," *Canadian Geotechnical Journal*, vol. 44, no. 7, pp. 765–780, 2007.

[2] R. Q. Huang, "Some catastrophic landslides since the twentieth century in the southwest of China," *Landslides*, vol. 6, no. 1, pp. 69–81, 2009.

[3] Q. Xu, X. M. Fan, R. Q. Huang et al., "A catastrophic rockslide-debris flow in Wulong, Chongqing, China in 2009: background, characterization, and causes," *Landslides*, vol. 7, no. 1, pp. 75–87, 2010.

[4] S. Xiong, W. Shi, Y. Wang, C. Zhu, and X. Yu, "Deformation and failure process of slope caused by underground mining: a case study of Pusa collapse in Nayong County, Guizhou Province, China," *Geofluids*, vol. 2022, Article ID 1592703, 19 pages, 2022.

[5] Y. Yin, P. Sun, M. Zhang, and B. Li, "Mechanism on apparent dip sliding of oblique inclined bedding rockslide at Jiweishan, Chongqing, China," *Landslides*, vol. 8, no. 1, pp. 49–65, 2011.

[6] M. Marschalko, I. Yilmaz, M. Bednárik, and K. Kubečka, "Variations in the building site categories in the underground mining region of Doubrava (Czech Republic) for land use planning," *Engineering Geology*, vol. 122, no. 3-4, pp. 169–178, 2011.

[7] Y. Zheng, C. X. Chen, T. T. Liu, H. Zhang, K. Xia, and F. Liu, "Study on the mechanisms of flexural toppling failure in anti-inclined rock slopes using numerical and limit equilibrium models," *Engineering Geology*, vol. 237, pp. 116–128, 2018.

[8] Z. Jianjun, W. Xun, S. Yanbing, W. Jiangbo, and M. L. Lee, "Deformation behavior of mining beneath flat and sloping terrains in mountainous areas," *Geofluids*, vol. 2021, Article ID 6689966, 16 pages, 2021.

[9] E. F. Salmi, M. Nazem, and M. Karakus, "Numerical analysis of a large landslide induced by coal mining subsidence," *Engineering Geology*, vol. 217, pp. 141–152, 2017.

[10] Y. B. Ning, H. M. Tang, F. Wang, and G. Zhang, "Sensitivity analysis of toppling deformation for interbedded anti-inclined rock slopes based on the Grey relation method," *Bulletin of Engineering Geology and the Environment*, vol. 78, no. 8, pp. 6017–6032, 2019.

[11] N. Abderahman, "Evaluating the influence of rate of undercutting on the stability of slopes," *Bulletin Engineering Geology and the Environment*, vol. 66, no. 3, pp. 303–309, 2007.

[12] F. Zhang, G. Liu, W. Chen, S. Liang, R. Chen, and W. Han, "Human-induced landslide on a high cut slope: a case of repeated failures due to multi-excavation," *Journal of Rock Mechanics and Geotechnical Engineering*, vol. 4, no. 4, pp. 367–374, 2012.

[13] T. N. Do and J. H. Wu, "Simulating a mining-triggered rock avalanche using DDA: a case study in Nattai North, Australia," *Engineering Geology*, vol. 264, article 105386, p. 14, 2020.

[14] B. Ghabraie, G. Ren, J. Barbato, and J. V. Smith, "A predictive methodology for multi-seam mining induced subsidence," *International Journal of Rock Mechanics and Mining Sciences*, vol. 93, pp. 280–294, 2017.

[15] Y. Cai, T. Verdel, and O. Deck, "On the topography influence on subsidence due to horizontal underground mining using the influence function method," *Computers and Geotechnics*, vol. 61, pp. 328–340, 2014.

[16] A. K. Alzo'ubi, C. D. Martin, and D. M. Cruden, "Influence of tensile strength on toppling failure in centrifuge tests," *International Journal of Rock Mechanics and Mining Sciences*, vol. 47, no. 6, pp. 974–982, 2010.

[17] Z. P. Yang, Q. Zhao, X. R. Liu, Z. Yin, Y. Zhao, and X. Li, "Experimental study on the movement and failure characteristics of karst mountain with deep and large fissures induced by coal seam mining," *Rock Mechanics and Rock Engineering*, vol. 55, no. 8, pp. 4839–4867, 2022.

[18] Y. Ning, H. Tang, G. Zhang et al., "A complex rockslide developed from a deep-seated toppling failure in the upper Lancang River, Southwest China," *Engineering Geology*, vol. 293, article 106329, 2021.

[19] L. Jing and O. Stephansson, *Fundamentals of Discrete Element Methods for Rock Engineering: Theory and Applications*, Elsevier, 2007.

[20] G. Shi, *Discontinuous Deformation Analysis: A New Numerical Model for the Statics and Dynamics of Block Systems, [Ph.D. Thesis]*, UC Berkeley, USA, 1988.

[21] P. A. Cundall and O. D. Strack, "A discrete numerical model for granular assemblies," *Geotechnique*, vol. 29, no. 1, pp. 47–65, 1979.

[22] F. Cui, C. Xiong, Q. Wu et al., "Dynamic response of the Daguangbao landslide triggered by the Wenchuan earthquake with a composite hypocenter," *Geomatics, Natural Hazards and Risk*, vol. 12, no. 1, pp. 2170–2193, 2021.

[23] H. Sarfaraz, "Stability analysis of flexural toppling failure using the Sarma's method," *Geotechnical and Geological Engineering*, vol. 38, no. 4, pp. 3667–3682, 2020.

[24] M. Havaej, D. Stead, E. Eberhardt, and B. R. Fisher, "Characterization of bi-planar and ploughing failure mechanisms in footwall slopes using numerical modelling," *Engineering Geology*, vol. 178, pp. 109–120, 2014.

[25] M. Azarafza, H. Akgün, A. Ghazifard, and E. Asghari-Kaljahi, "Key-block based analytical stability method for discontinuous rock slope subjected to toppling failure," *Computers and Geotechnics*, vol. 124, article 103620, 2020.

[26] M. Bahaaddini and M. Rahimi, "Distinct element modelling of the mechanical behaviour of intact rocks using voronoi tessellation model," *International Journal of Mining and Geo-Engineering*, vol. 52, no. 1, pp. 61–68, 2018.

[27] G. Ma, X. W. Hu, Y. P. Yin, G. Luo, and Y. Pan, "Failure mechanisms and development of catastrophic rockslides triggered by precipitation and open-pit mining in Emei, Sichuan, China," *Landslides*, vol. 15, no. 7, pp. 1401–1414, 2018.

[28] S. Y. Li, D. D. Li, H. D. Liu, S. W. Wang, Z. Geng, and B. Peng, "Formation and failure mechanism of the landslide: a case study for Huaipa, Western Henan, China," *Environmental Earth Science*, vol. 80, no. 15, article 478, pp. 1–12, 2021.

[29] J. Zhao, J. Xiao, M. L. Lee, and Y. Ma, "Discrete element modeling of a mining-induced rock slide," *SpringerPlus*, vol. 5, no. 1, article 1633, pp. 1–19, 2016.

[30] F. Zhen, L. Bin, C. Q. Peng, and C. J. Wen, "Initiation mechanism of the Jiweishan landslide in Chongqing, southwestern China," *Environmental & Engineering Geoscience*, vol. 22, no. 4, pp. 341–351, 2016.

[31] J. H. Liu and W. T. Ding, "Optimal study of reinforcement on a karst slope of Shui-Nan highway," *Advanced Materials Research*, vol. 433-440, pp. 345–348, 2012.

[32] D. Martin, "Deformation of open pit mine slopes by deep seated toppling," *International Journal of Surface Mining, Reclamation and Environment*, vol. 4, no. 4, pp. 153–164, 1990.

[33] D. Ma, H. Y. Duan, J. X. Zhang, X. Liu, and Z. Li, "Numerical simulation of water–silt inrush hazard of fault rock: a three-phase flow model," *Rock Mechanics and Rock Engineering*, vol. 55, no. 8, pp. 5163–5182, 2022.

[34] D. Ma, H. Y. Duan, and J. X. Zhang, "Solid grain migration on hydraulic properties of fault rocks in underground mining tunnel: radial seepage experiments and verification of permeability prediction," *Tunnelling and Underground Space Technology*, vol. 126, article 104525, 2022.

[35] Q. Li, D. Ma, Y. Zhang, Y. Liu, Y. Ma, and D. Hu, "Insights into controlling factors of pore structure and hydraulic properties of broken rock mass in a geothermal reservoir," *Lithosphere*, vol. 2022, article 3887832, 17 pages, 2022.

[36] X. M. Fan, Q. Xu, G. Scaringi et al., "The "long" runout rock avalanche in Pusa, China, on August 28, 2017: a preliminary report," *Landslides*, vol. 16, no. 1, pp. 139–154, 2019.

[37] Y. Zhu, S. Xu, Y. Zhuang, X. Dai, G. Lv, and A. Xing, "Characteristics and runout behaviour of the disastrous 28 August 2017 rock avalanche in Nayong, Guizhou, China," *Engineering Geology*, vol. 259, article 105154, 2019.

[38] L. Chen, C. Zhao, Y. Kang et al., "Pre-event deformation and failure mechanism analysis of the Pusa landslide, China with multi-sensor SAR imagery," *Remote Sensing*, vol. 12, no. 5, p. 856, 2020.

[39] M. A. Pritchard and K. W. Savigny, "Numerical modelling of toppling," *Canadian Geotechnical Journal*, vol. 27, no. 6, pp. 823–834, 1990.

[40] F. Cui, B. Li, C. Xiong et al., "Dynamic triggering mechanism of the Pusa mining-induced landslide in Nayong County, Guizhou Province, China," *Geomatics, Natural Hazards and Risk*, vol. 13, no. 1, pp. 123–147, 2021.

[41] L. Q. Chen, C. Y. Zhao, B. Li et al., "Deformation monitoring and failure mode research of mining-induced Jianshanying landslide in karst mountain area, China with ALOS/PAL-SAR-2 images," *Landslides*, vol. 18, no. 8, pp. 2739–2750, 2021.

[42] Z. Q. Chang, W. Yu, W. Wang, J. Zhang, X. Liu, and J. Zhu, "An approach for accurately retrieving the vertical deformation component from two-track InSAR measurements," *International Journal of Remote Sensing*, vol. 38, no. 6, pp. 1702–1719, 2017.

[43] P. Li, C. R. Liang, Z. H. Li, C. Shi, and J. N. Liu, "Recent advances on the earthquake and volcanic deformation monitoring with wide-swath InSAR observations," *Progress in Geophysics*, vol. 30, no. 4, pp. 1597–1607, 2015.